SCIENTIFIC REP⚙RTS

OPEN

Lateral-drag propulsion forces induced by anisotropy

Igor S. Nefedov[1,2] & J. Miguel Rubi[3]

We predict the existence of lateral drag forces near the flat surface of an absorbing slab made of an anisotropic material. The forces originate from the fluctuations of the electromagnetic field, when the anisotropy axis of the material forms a certain angle with the surface. In this situation, the spatial spectra of the fluctuating electromagnetic fields becomes asymmetric, different for positive and negative transverse wave vectors components. Differently from the case of van der Waals interactions in which the forward-backward symmetry is broken due to the particle movement, in our case the lateral motion results merely from the anisotropy of the slab. This new effect, of particular significance in hyperbolic materials, could be used for the manipulation of nanoparticles.

Fluctuating electromagnetic fields are responsible for important phenomena such as thermal emission, radiative heat transfer, van der Waals interactions, Casimir effect, and van der Waals friction between bodies[1]. The existence of attractive forces between two perfectly conducting parallel plates, induced by vacuum fluctuations at zero temperature, was predicted by Casimir in 1948[2,3] and subsequently by Lifshitz[4] for any media at finite temperature. A general electromagnetic fluctuation theory, referred to as fluctuational electrodynamics, was proposed by Rytov in 1950[5]. The conventional Casimir force between two parallel surfaces is orthogonal to the surfaces, of attractive or repulsive nature depending on the separation distance and on the medium filling the gap between surfaces[6,7].

The lateral component of the Poynting vector, integrated over the whole spatial spectrum, vanishes near flat surfaces because its positive and negative components balance each other out. This symmetry can be broken by a mutual lateral movement of the bodies, as happens in the case of contact-free van der Waals and quantum friction[8,9]. To observe these forces, one applies an electric current to a conducting layer and measures the friction drag effect of electrons in a second parallel metallic layer[10,11]. Lateral drag forces can also be present nearby surface inhomogeneities, such as corrugations[12–14]. These forces, however, can only give rise to local displacements that follow the periodicity of the corrugations[15–17] and not to a net movement of the particle over an appreciable distance. A lateral propulsion force, exerted on an anisotropic particle in a non-equilibrium regime, was predicted by Müller and Krüger[18]. In the situation analyzed, the forces acting on the particle cause not only lateral motion but also rotation leading the particle to a state of minimal energy where lateral motion ceases. Anisotropy can also induce van der Waals torques, predicted between anisotropic half-spaces[19], anisotropic cylinders[20], and other objects. For more details see the review article[14].

In this work, we propose a new mechanism able to generate lateral forces not subjected to the restriction of local motion imposed by surface corrugations. The force is induced by fluctuations of the electromagnetic field and not by quantum (zero field) fluctuations. If the absorbing medium is anisotropic and the anisotropy axis is tilted with respect to the slab surface, absorption of the TM-polarized wave incident on the slab is different for positive and negative incident angles, although the reflection be the same[21,22]. The net force induced moves the particle in a direction parallel to the surface.

To calculate the lateral force, we solved the boundary-value problem for electromagnetic waves, excited by point-like fluctuating currents within a finite-thickness slab of an anisotropic medium (see Fig. 1). The correlations of the current are given by fluctuating electrodynamics[5]. Due to the homogeneity of the considered geometry in the x and y directions, the electric and magnetic fields and the current can be represented by means of their corresponding Fourier transforms $\mathbf{E}(\omega, k_x, k_y)$, $\mathbf{H}(\omega, k_x, k_y)$, and $\mathbf{j}(\omega, k_x, k_y)$. To find a fully accurate solution of the electromagnetic fields is a difficult task because the fields in the considered geometry cannot be decomposed into TM and TE waves. To show the existence of a lateral force, however, it is enough to consider TM waves propagating along the slab in the anisotropy plane, assuming $k_y = 0$.

[1]Aalto University, School of Electrical Engineering, P.O. Box 13000, 00076, Aalto, Finland. [2]Laboratory Nanooptomechanics, ITMO University, St. Petersburg, 197101, Russia. [3]Statistical and Interdisciplinary Physics Section, Departament de Fisica de la Matèria Condensada, Universitat de Barcelona, Marti i Franquès 1, 08028, Barcelona, Spain. Correspondence and requests for materials should be addressed to J.M.R. (email: mrubi@ub.edu)
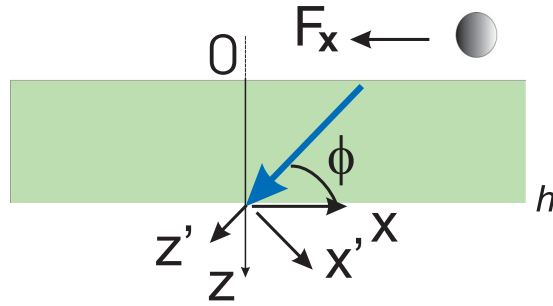
Figure 1. The anisotropic slab and the small particle affected by the lateral force. The anisotropy axis, indicated by a thick blue arrow, forms an angle ϕ with the slab interface. Its thickness is h. Reference frames (x, y, z) and (x', y', z') are associated with the slab interface and the anisotropy axis, respectively. The black arrow shows the direction of motion of the particle due to the action of the x-component of the radiative forces $\mathbf{F}_x$.

The article is organized as follows. In section II, we solve the boundary value problem for electromagnetic waves propagating in the anisotropic slab and calculate the normal and lateral components of the Poynting vector. In Section III, we obtain the eigenwaves. Section IV is devoted to the calculation of the radiative force on a dipole particle. Finally, in Section V, we present our results for the lateral force.

Normal and lateral components of the Poynting vector

In the coordinate system (x', y', z') (see Fig. 1) the relative permittivity tensor has the diagonal form

$$\bar{\bar{\epsilon}}' = \epsilon_\parallel \mathbf{z}'_0 \mathbf{z}'_0 + \epsilon_t (\mathbf{x}'_0 \mathbf{x}'_0 + \mathbf{y}'_0 \mathbf{y}'_0). \tag{1}$$

where the subscript 0 denotes unit vector. The components of the permittivity tensor in the reference frame x, y, z, associated with the slab interface $\bar{\bar{\epsilon}}$ are the following[21]:

$$\begin{aligned}
\epsilon_{xz} &= \epsilon_{zx} = (\epsilon_\parallel - \epsilon_t)\cos\phi\,\sin\phi \\
\epsilon_{xx} &= \epsilon_\parallel \sin^2\phi + \varepsilon_t \cos^2\phi \\
\epsilon_{zz} &= \epsilon_\parallel \cos^2\phi + \varepsilon_t \sin^2\phi.
\end{aligned} \tag{2}$$

If the anisotropy axis is tilted with respect to the slab interfaces, the Maxwell equations can be split up into TM and TE subsystems, provided that the wave vector lies in the anisotropy axis plane or is orthogonal to it. We will restrict our analysis to TW waves.

The propagation constants of those waves, travelling along the z-direction for a fixed k_x are given by[21]

$$k_z^{(1,2)} = \frac{-k_x \epsilon_{xz} \pm \sqrt{(\epsilon_{xz}^2 - \epsilon_{xx}\epsilon_{zz})(k_x^2 - k_0^2 \epsilon_{zz})}}{\epsilon_{zz}}. \tag{3}$$

where k_0 is the wavenumber in vacuum. The transverse wave impedances $Z_{1,2}$, connecting tangential field components, reads as[21]

$$Z_{1,2} = \frac{E_x}{H_y} = \pm \frac{\eta}{k_0} \frac{\sqrt{k_x^2 - k_0^2 \epsilon_{zz}}}{\sqrt{\epsilon_{xz}^2 - \epsilon_{xx}\epsilon_{zz}}}, \tag{4}$$

where $\eta = 120\pi$ Ohm is the wave impedance of vacuum.

For the tangential field components $\mathrm{X}(z) = (E_x(z), H_y(z))$, excited by the fluctuating currents $j_x(z)$, $j_z(z)$ located within the absorptive layer $0 < z < h$ (see Fig. 1), the Maxwell equations reduce to the system of two ordinary differential equations:

$$\frac{d}{dz}\mathrm{X}(z) = [A]\mathrm{X}(z) + \mathrm{F}(z) \tag{5}$$

where the matrix elements of $[A]$ are given by

$$\begin{aligned}
A_{11} &= -i\frac{k_x \epsilon_{xz}}{\epsilon_{zz}}, &\quad A_{12} &= i\eta k_0 \left(1 - \frac{k_x^2}{k_0^2 \epsilon_{zz}}\right) \\
A_{21} &= i\frac{k_0}{\eta}\left(\epsilon_{xx} - \frac{\epsilon_{xz}^2}{\epsilon_{zz}}\right), &\quad A_{22} &= -ik_x \frac{\epsilon_{xz}}{\epsilon_{zz}}
\end{aligned} \tag{6}$$

and the components of the vector $\mathrm{F}(z) = (F_1(z), F_2(z))$ are

$$F_1(z) = \eta \frac{k_x}{k_0 \epsilon_{zz}} j_z(z) = a j_z(z),$$

$$F_2(z) = \frac{\epsilon_{xz}}{\epsilon_{zz}} j_z(z) - j_x(z) = b j_z(z) - j_x(z),$$

(7)

The elementary bulk current source has the form: $\mathbf{j}(z) = \mathbf{j}_0(z')\delta(z - z')$.

The solution of Eq. (5) for points $0 < z < h$ is[23]:

$$X(z) = e^{[A]z} X(0) + \int_0^z e^{[A](z-\tau)} F(\tau) d\tau,$$

(8)

with $[M(z)] = e^{[A]z}$ the transfer matrix. Expressions for the two-by-two matrix components, for the case in which the wave impedances and vector components are different for waves propagating in opposite directions, are given in refs 21, 22. For the considered case, where $Z_2 = -Z_1 = Z$, those expressions reduce to

$$M_{11}(z) = \frac{1}{2}[e^{ik_{z1}z} + e^{ik_{z2}z}] \quad M_{12}(z) = \frac{Z}{2}[e^{ik_{z1}z} - e^{ik_{z2}z}]$$

$$M_{21}(z) = \frac{1}{Z}[e^{ik_{z1}z} - e^{ik_{z2}z}] \quad M_{22}(z) = M_{11}(z).$$

(9)

The boundary conditions are: $X_2(0) = X_1(0)/Z_0$, $X_2(h) = -X_1/Z_0$, where $Z_0 = \eta\sqrt{(k_0^2 - k_x^2)}/k_0$ is the *transverse wave impedance* in vacuum. We can then express the tangential field components at the interface $x = 0$, created by a current located at z' in the form

$$X_1(0,z') = \frac{1}{\Delta} \int_0^h \left[U(\tau) j_{x0}(z') + V(\tau) j_{z0}(z')\right] \delta(\tau - z') \, d\tau = \frac{1}{\Delta}\left[U(z') j_{x0}(z') + V(z') j_{z0}(z')\right],$$

(10)

where

$$\Delta = M_{11}(h) + M_{22}(h) - M_{12}(h)/Z_0 - M_{21}(h)Z_0,$$
$$U(\tau) = M_{12}(h - \tau) - Z_0 M_{22}(h - \tau),$$
$$V(\tau) = a[Z_0 M_{21}(h - \tau) - M_{11}(h - \tau)] + b[Z_0 M_{22}(h - \tau) - M_{12}(h - \tau)].$$

(11)

The Fourier components of the electric and magnetic fields out of the layer are given by

$$E_x(k_x, z, z') = \begin{cases} X_1(0, z')e^{-ik_{z0}z}, & z < 0, \\ X_1(h, z')e^{ik_{z0}(z-h)}, & z > h, \end{cases}$$

(12)

where $k_{z0} = \sqrt{k_0^2 - k_x^2}$ and $H_y(k_x, z, z') = E_x(k_x, z, z')/Z_0$. For evanescent waves, $|k_x| > k_0$, we have to take $k_{z0} = -i|k_{z0}|$, if $z < 0$ and $k_{z0} = i|k_{z0}|$, if $z > h$.

The average values of the fluctuating currents vanish, only their correlations contribute to the energy flux. These correlations are given through the fluctuation-dissipation theorem[24] The ensemble-averaged Poynting vector in the plane $z = 0$, for the k_x mode, induced by fluctuating currents located within the slab, $0 < z', z'' < h$, reads

$$\langle S_z(\omega, k_x) \rangle = \frac{1}{2} \int_0^h \int_0^h \left\langle E_x(k_x, z') H_y^*(k_x, z'') \right\rangle dz' dz'',$$

(13)

where the correlation $\left\langle E_x(k_x, z') H_y^*(k_x, z'') \right\rangle$ is obtained by using the fluctuation-dissipation theorem[24]

$$\langle j_m(\mathbf{r}, \omega) j_n^*(\mathbf{r}', \omega') \rangle = \frac{4}{\pi} \omega \epsilon_0 \epsilon_{mn}''(\omega) \delta(\mathbf{r} - \mathbf{r}') \delta(\omega - \omega') \Theta(\omega, T),$$

(14)

with $\overrightarrow{r} = (x, z)$ and

$$\Theta(\omega, T) = \frac{\hbar\omega}{e^{\hbar\omega/(k_B T)} - 1}$$

(15)

the Planck's oscillator energy. Contribution from vacuum fluctuations is omitted since thermal fluctuations only contribute to the lateral forces. In Eq. (14), $\epsilon_{mn}'' \equiv \text{Im}(\epsilon_{mn})$, ϵ_0 is the permittivity of vacuum, $\hbar$ the reduced Planck constant, T the temperature, and k_B the Boltzmann constant.

Using the fluctuation-dissipation theorem (14), we then obtain

$$\langle S_z(\omega, k_x) \rangle = \frac{4\omega\epsilon_0 \Theta(\omega, T)}{2\pi |\Delta|^2 Z_0^*}[D_1 \epsilon_{xx}'' + D_2 \epsilon_{zz}'' + D_3 \epsilon_{xz}''],$$

(16)

where we have defined the coefficients

$$D_1 = \int_0^h U(\tau)U^*(\tau)d\tau,$$

$$D_2 = \int_0^h V(\tau)V^*(\tau)d\tau,$$

$$D_3 = \int_0^h U(\tau)V^*(\tau)d\tau + c.\,c,$$

(17)

The expressions for these coefficients are found to be

$$D_1 = \frac{1}{4}\left\{\frac{i\,|Z-Z_0|^2}{(k_{z1}-k_{z1}^*)}(1-e^{i(k_{z1}-k_{z1}^*)h}) + \frac{i\,|Z+Z_0|^2}{(k_{z2}-k_{z2}^*)}(1-e^{i(k_{z2}-k_{z2}^*)h})\right.$$
$$\left. -\left[\frac{i(Z-Z_0)(Z^*+Z_0^*)}{(k_{z1}-k_{z2}^*)}(1-e^{i(k_{z1}-k_{z2}^*)h}) + c.\,c.\right]\right\}.$$

(18)

$$D_2 = \frac{|a|^2}{4}\left\{\frac{i\,|Z_0/Z-1|^2}{(k_{z1}-k_{z1}^*)}(1-e^{i(k_{z1}-k_{z1}^*)h}) + \frac{i\,|Z_0/Z+1|^2}{(k_{z2}-k_{z2}^*)}(1-e^{i(k_{z2}-k_{z2}^*)h})\right.$$
$$\left. + -\left[\left[\frac{i(Z_0/Z-1)(Z_0^*/Z^*+1)}{(k_{z1}-k_{z2}^*)}(1-e^{i(k_{z1}-k_{z2}^*)h}) + c.\,c.\right]\right]\right\}$$
$$+\frac{|b|^2}{4}\left\{\frac{i\,|Z_0-Z|^2}{(k_{z1}-k_{z1}^*)}(1-e^{i(k_{z1}-k_{z1}^*)h}) + \frac{i\,|Z_0+Z|^2}{(k_{z2}-k_{z2}^*)}(1-e^{i(k_{z2}-k_{z2}^*)h})\right.$$
$$\left. +\left[\frac{i(Z_0-Z)(Z_0^*+Z^*)}{(k_{z1}-k_{z2}^*)}(1-e^{i(k_{z1}-k_{z2}^*)h}) + c.\,c.\right]\right\}$$
$$+\left\{\frac{ab^*}{4Z}\left[\frac{i\,|Z_0-Z|^2}{k_{z1}-k_{z1}^*}(1-e^{i(k_{z1}-k_{z1}^*)h}) - \frac{i\,|Z_0+Z|^2}{k_{z2}-k_{z2}^*}(1-e^{i(k_{z2}-k_{z2}^*)h})\right.\right.$$
$$+\frac{i(Z_0-Z)(Z_0^*+Z^*)}{k_{z1}-k_{z2}^*}(1-e^{i(k_{z1}-k_{z2}^*)h})$$
$$\left.\left. -\frac{i(Z_0+Z)(Z_0^*-Z^*)}{k_{z2}-k_{z1}^*}(1-e^{i(k_{z2}-k_{z1}^*)h})\right] + c.\,c.\right\}.$$

(19)

$$D_3 = \frac{1}{4}\left[\frac{iC_1(Z-Z_0)}{k_{z1}-k_{z1}^*}(1-e^{i(k_{z1}-k_{z1}^*)h}) + \frac{iC_2(Z+Z_0)}{k_{z2}-k_{z2}^*}(1-e^{i(k_{z2}-k_{z2}^*)h})\right.$$
$$\left. -\frac{iC_2(Z-Z_0)}{k_{z1}-k_{z2}^*}(1-e^{i(k_{z1}-k_{z2}^*)h}) - \frac{iC_1(Z+Z_0)}{k_{z2}-k_{z1}^*}(1-e^{i(k_{z2}-k_{z1}^*)h})\right],$$

(20)

with

$$C_1 = a^*Z_0^*/Z - a^* + b^*Z_0^* - b^*Z^*,$$
$$C_2 = a^*Z_0^*/Z + a^* - b^*Z_0^* - b^*Z^*.$$

(21)

If the anisotropy axis is parallel or orthogonal to the interface, then $\langle S_z(\omega, k_x)\rangle = \langle S_z(\omega, -k_x)\rangle$. Otherwise, that average becomes asymmetric with respect to the normal to the slab interface, as occurs in absorption[21, 22]. This value is real if $|k_x| < k_0$ and imaginary if $|k_x| > k_0$. Actually, the real part of $\langle S_z(\omega, k_x)\rangle$ determines the far-field thermal emission at the angle $\theta = arcsin\, k_x/k_0$.

Outside the slab, the lateral time-averaged component of the Poynting vector is given by

$$\langle S_x(\omega, k_x, z)\rangle = -\frac{1}{2}E_zH_y^* = \frac{k_x}{k_{z0}}\langle S_z(\omega, k_x)\rangle f(z),$$

(22)

where $f(z) = 1$, if $|k_x| < k_0$, and $f(z) = e^{2|k_{z0}|z}$ $(z < 0)$, if $|k_x| > k_0$. Unlike $\langle S_z(\omega, k_x)\rangle$, this value is real for all k_x, i.e. both for propagating and evanescent waves. The contribution of all k_x-modes to the x-component of the Poynting vector outside the slab is given as:

$$\langle S_x(\omega)\rangle = \frac{1}{2\pi}\int_{-\infty}^{\infty}\langle S_x(\omega, k_x, z)\rangle dk_x.$$

(23)

Despite the fact that the lateral component of the Poynting vector is real for all k_x, propagating waves only give contribution to the overall value (23), hence $\langle S_x(\omega, k_x, z)\rangle \neq \langle S_x(\omega, -k_x, z)\rangle$, if $|k_x| < k_0$ and $\langle S_x(\omega, k_x, z)\rangle = \langle S_x(\omega,$

$-k_x, z)\rangle$, if $|k_x| \geq k_0$. These results come from the fact that the field correlators outside a finite-thickness slab of an absorbing medium are expressed via transmission and reflection coefficients for the propagating waves spectrum and via reflection coefficients only for evanescent waves (see, for example[25], Eq. (120), and ref. [26], Eq. (103)). For the slab made of an anisotropic material with a tilted anisotropy axis the reflection coefficients are symmetric with respect to $\pm k_x$ for any k_x, whereas the transmission coefficients are asymmetric.

Since $\langle S_x(\omega, k_x, z)\rangle \neq \langle S_x(\omega, -k_x, z)\rangle$ ($|k_x| < k_0$), one can expect the appearance of radiative forces dragging a particle placed nearby the slab along its surface.

When $|k_x| < k_0$, expression (13) gives us the thermal power radiating from the slab in the anisotropy axis (x, z) plane, i.e. for $k_y = 0$. The total energy flux density in the x-direction, produced by electromagnetic fluctuations, is given by

$$\langle S_x(z)\rangle^{\text{tot}} = \int_0^\infty \frac{d\omega}{(2\pi)^3} \int\int_{-k_0}^{k_0} \langle S_x(\omega, k_x, k_y)\rangle dk_x dk_y. \tag{24}$$

An exact value of this quantity for nonzero values of k_x and k_y is difficult to obtain since the fluctuating fields in the slab are carried by hybrid waves whose solution is more difficult to obtain than that for TM waves.

The calculation of the total energy flux in the x-direction is based on the following consideration. If the anisotropy axis is orthogonal to the slab interfaces or if the medium is isotropic, due to azimuthal symmetry, one can replace $dk_x dk_y$ by $2\pi k_x dk_x$, therefore

$$\int_{-k_0}^{k_0}\int_{-k_0}^{k_0} \langle S_z(\omega, k_x, k_y)\rangle dk_x \, dk_y = 2\pi \int_0^{k_0} \langle S_z(\omega, q)\rangle q \, dq \tag{25}$$

and $\langle S_x(z)\rangle^{\text{tot}} = \langle S_x^s(z)\rangle + \langle S_x^p(z)\rangle \equiv 0$. Let us consider separately the cases in which the wave vector is either parallel or orthogonal to the plane normal to the slab surface, containing the anisotropy axis. In both cases, waves in an anisotropic slab can be split up into p-polarized and s-polarized waves. Obviously, for the s-polarized waves the asymmetry never takes place and $\langle S_x^p(z)\rangle \equiv 0$ for both cases, $k_x \neq 0$, $k_y = 0$ and $k_x = 0$, $k_y \neq 0$. For p-polarized waves, the asymmetry is absent if $k_x = 0$, at any k_y and it is maximal if $k_x \neq 0$, $k_y = 0$. Thus, the integral over waves, propagating in the y-direction, i.e. $k_x = 0$, gives zero contribution to $\langle S_c^p(z)\rangle$. A good approximation to the total lateral energy flux density is then given by

$$\langle S_x^{\text{appr}}(z)\rangle^{\text{tot}} \approx \frac{1}{4\pi} \int_0^\infty d\omega \int_{-k_0}^{k_0} \langle S_x^p(\omega, q)\rangle q \, dq. \tag{26}$$

Asymmetry with respect to $\pm k_x$ takes place for any absorbing anisotropic material but it becomes particularly important for media characterized by hyperbolic dispersion, for the so-called *hyperbolic materials*, whose diagonal components of the permittivity tensor have different signs. To illustrate the lateral drag effect, we will consider the orthorhombic modification of boron nitride which exhibits hyperbolic dispersion in certain frequency ranges[27, 28].

The Lorentzian model and the eigenwaves in a boron nitride medium

The components of the permittivity tensor are given by the Lorentz model[27, 28]:

$$\epsilon_{\parallel,\perp} = \epsilon_{\parallel,\perp}^\infty + \frac{U_{\parallel,\perp}(\omega_{\parallel,\perp}^\tau)^2}{(\omega_{\parallel,\perp}^\tau)^2 - \omega^2 - i\omega\Gamma_{\parallel,\perp}}, \tag{27}$$

where $\omega_{\parallel,\perp}^\tau$ and $U_{\parallel,\perp}$ are, respectively, the transverse phonon frequency and the oscillator strength of the lattice vibration for the parallel and perpendicular polarizations, and $\Gamma_{\parallel,\perp}$ is the damping constant. The constants $\epsilon_{\parallel,\perp}^\infty$ are the components of the permittivity tensor at frequencies ω that greatly exceed the phonon resonance frequency $\omega_{\parallel,\perp}^\tau$. The values of the parameters of (27) used are: $\epsilon_\parallel^\infty = 2.7$, $U_\parallel = 0.48$, $\omega_\parallel^\tau = 1.435 \times 10^{14}$ rad/s, $\Gamma_\parallel = 8.175 \times 10^{11}$ rad/s, $\epsilon_\perp^\infty = 5.2$, $U_\perp = 2$, $\omega_\perp^\tau = 2.588 \times 10^{14}$ rad/s, $\Gamma_\perp = 1.29 \times 10^{12}$ rad/s. For this parameters, the Lorentzian resonances of $\epsilon_\parallel$ and $\epsilon_\perp$, take place at frequencies $\approx$22.8 THz and $\approx$41.2 THz, respectively.

The propagation constants and the transverse wave impedance of the TM waves, traveling along the z-direction under fixed k_x, are given by Eqs (3) and (4), respectively. In order to correctly identify the waves propagating in the positive and negative directions of the z-axis, we have to analyze the imaginary parts of $k_z^{(1,2)}$, according to the causality principle. Let us define the normal wave vector component for the downward wave (propagating in the positive z-direction) as k_1 and for the upward wave as k_2. One then has: Im $(k_1) > 0$ and Im $(k_2) < 0$. The parallel $\epsilon_\parallel$ and perpendicular $\epsilon_\perp$ components of the permittivity tensor of orthorhombic boron nitride, taken for illustration of the predicted effect, exhibit the Lorentzian resonances at frequencies $\approx$22.8 THz and $\approx$41.2 THz, respectively. It is expected, that k_1 and k_2 exhibit a resonant behavior nearby these frequencies.

Figure 2 illustrates the frequency dependencies of the real and imaginary parts of the normal components k_1, k_2 of wave vectors. One can see that Re(k_1) changes the sign in the vicinity of the resonance, so the downward propagating wave becomes the forward wave at low frequencies and the backward wave in the frequency range from $\approx$23.6 THz to $\approx$25 THz. The upward wave remains the forward one within the considered range. Figure 3 shows similar dependencies on the frequency range around the $\epsilon_\perp$ resonance. Unlike the previous case, here the upward wave changes the sign of dispersion.
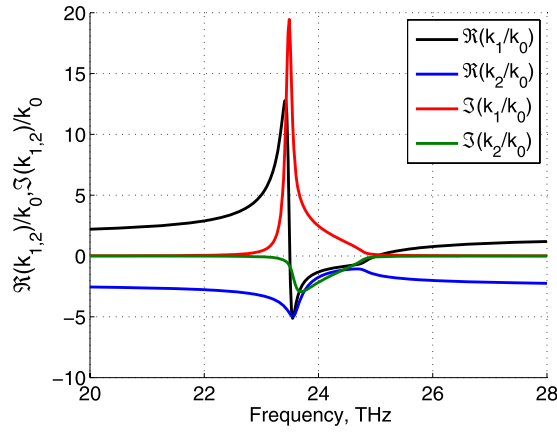
Figure 2. Real and imaginary parts of k_1 and k_2, normalized to the wavenumber in vacuum k_0, versus frequency in the vicinity of the $\epsilon_\parallel$- resonance.
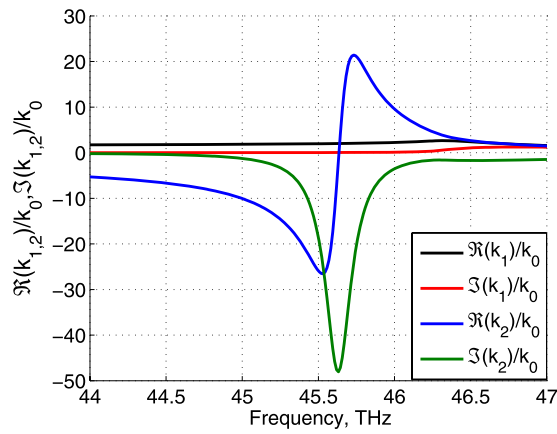

Figure 3. Real and imaginary parts of k_1 and k_2, normalized to the wavenumber in vacuum k_0, versus frequency in the vicinity of the $\epsilon_\perp$ - resonance.
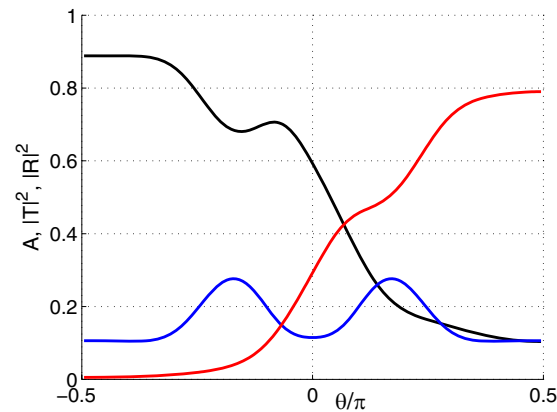

Figure 4. Absorption A (black), transmission $|T|^2$ (red) and reflection $|R|^2$(blue) of the plane wave incident onto the slab of orthorhombic boron nitride versus the incidence angle θ [rad]. The thickness of the layer h is 1.5 μm and the tilt angle $\phi = 40°$.

The dependence of the transmission, $|T|^2$, reflection, $|R|^2$, and absorption $A = 1 - |T|^2 - |R|^2$ on the incidence angle, calculated at 45 THz which is close to the Lorentzian resonance for $\epsilon_\parallel$, is shown in Fig. 4. The displayed dependence of the absorption versus the incidence angle is the signature of the asymmetry of thermal emission and radiative forces with respect to k_x.

Radiative forces on a dipole particle

To evaluate the effect of the lateral forces, we will consider a small particle moving under the influence of fluctuating electromagnetic fields. The dipolar force acting on the particle can be written as[29]

$$\langle \mathbf{F} \rangle = \frac{1}{4}\text{Re}\{\alpha\}\nabla|\mathbf{E}|^2 + \sigma\frac{1}{2}\text{Re}\left\{\frac{1}{c}\mathbf{E}\times\mathbf{H}^*\right\} + \sigma\frac{1}{2}\text{Re}\left\{i\frac{\epsilon_0}{k_0}(\mathbf{E}\cdot\nabla)\mathbf{E}^*\right\}$$

(28)

where α is the polarizability of the particle given by

$$\alpha = \frac{\alpha_0}{1 - i\alpha_0 k_0^3/(6\pi\epsilon_0)}, \quad \alpha_0 = 4\pi\epsilon_0 r^3\frac{\epsilon - 1}{\epsilon + 2},$$

(29)

with r and ϵ its radius and permittivity, respectively, and $\sigma = k_0\text{Im}\{\alpha\}/\epsilon_0$. The origin of the force is the presence of thermal fluctuations in the anisotropic slab which give rise to thermal emission from the slab into the far zone. Finite thickness of the slab and tilted anisotropy axis are conditions necessary to generate the force. Zero-field fluctuations do not give a contribution to the force since the energy flows incoming from the left and the right sides balance each other out.

The first term in (28), related to the gradient forces, causes attraction of the particle toward the slab interface due to the z-dependence of fields through $e^{|k_{z0}|z}$, for $z < 0$ (van-der-Waals forces[1]). The explicit expression for $\nabla|\mathbf{E}|^2$ is

$$\nabla|\mathbf{E}(\omega, k_x, z)|^2 = \frac{\partial}{\partial z}f(z)[\langle E_x E_x^*\rangle + \langle E_z E_z^*\rangle] = 2\langle S_z(\omega, k_x)\rangle\eta f(z)\frac{2k_x^2 - k_0^2}{k_0},$$

(30)

Only the evanescent waves ($|k_x| > k_0$) contribute to this force.

In the second contribution, the x- and z-component of the Poynting vector exert pulling forces along the corresponding directions. At small $|z|$, the attractive gradient force is dominant, whereas at larger $|z|$ the dominant force is the repulsive force proportional to the z component of the Poynting vector.

Due to the fact that

$$\langle(\mathbf{E}\cdot\nabla)\mathbf{E}^*\rangle_x = E_x\frac{\partial}{\partial x}E_x^* + E_z\frac{\partial}{\partial z}E_x^* = 0,$$

$$\langle(\mathbf{E}\cdot\nabla)\mathbf{E}^*\rangle_z = E_x\frac{\partial}{\partial x}E_z^* + E_z\frac{\partial}{\partial z}E_z^* = 0,$$

(31)

the third term in (28) does not contribute to the radiative forces. The x-component of the Poynting vector in (28) is given by Eq. (26) and the z-component can be found by replacing $\langle S_x^p(\omega, q)\rangle$ by $\langle S_z^p(\omega, q)\rangle = -(k_{z0}/k_x)\langle S_x^p(\omega, q)\rangle$.

Note, that since the TM (p)-polarized waves only contribute to the lateral Poynting vector at $k_y = 0$ and in our approximation we have not taken into account the hybrid nature of waves in the anisotropic slab at $k_y \neq 0$, we can consider contributions of the p-polarized waves only to the x-directed forces.

As an example of particle experiencing a lateral drag force, we consider a spherical nanoparticle, made of doped silicon, whose complex permittivity ϵ_s in the infrared and far infrared ranges can be calculated by using the Masetti model[30]. This model considers that the permittivity of heavily doped silicon is given by the Drude formula[30, 31]:

$$\epsilon(\omega) = \epsilon_\infty - \frac{\omega_p^2}{\omega(\omega - j\gamma)}$$

(32)

where $\epsilon_\infty \approx 11.6$ is the high-frequency limit value of the permittivity[32], and γ is the scattering rate which depends on the mobility of the carriers. The plasma frequency and scattering rate are expressed as $\omega_p = \sqrt{Ne^2/(m^*\epsilon_0)}$ and $\gamma = e/(m^*\mu)$, respectively, where e is the electron charge, N is the carrier concentration, m^* is the carrier effective mass, and μ is the mobility. For n-type heavily doped Si, the mobility expression is given as[31]

$$\mu = \mu_1 + \frac{\mu_{max} - \mu_1}{1 + (N/C_r)^\alpha} - \frac{\mu_2}{1 + (C_s/N)^\beta}.$$

(33)

Here $m^* = 0.27m_0$, where m_0 is the electron mass, $\mu_1 = 68.5\,\text{cm}^2/\text{V s}$, $\mu_{max} = 1414\,\text{cm}^2/\text{V s}$, $\mu_2 = 56.1\,\text{cm}^2/\text{V s}$, $C_r = 9.2\times10^{17}\,\text{cm}^{-3}$, $C_s = 3.42\times10^{20}\,\text{cm}^{-3}$, $\alpha = 0.711$ and $\beta = 1.98$. For these parameters, $\omega_p = 1.084\times10^{15}\,\text{rad/s}$ and $\gamma = 8.586\times10^{13}\,\text{rad/s}$. The concentration of carriers is $9\times10^{19}\,\text{cm}^{-3}$ and its radius 15 nm. For these values of the parameters the particle exhibits a dipole resonance within the same frequency range as for the perpendicular component of the permittivity tensor of orthorhombic boron nitride, namely, around 44 THz, see Fig. 5. In the figure, one can see a very strong enhancement of Im (α), proportional to the lateral force, within the frequency band, providing main contribution to the lateral component of the Poynting vector.

Results and Discussion

Figure 6 shows the dipolar forces acting on the particle, computed at $z = 1\,\mu m$, and integrated in frequencies. The lower integration limit is 20 THz since below this frequency contributions to all radiative forces are very small. The upper limit corresponds to a current frequency at the abscissa axis. One can see that the main contributions
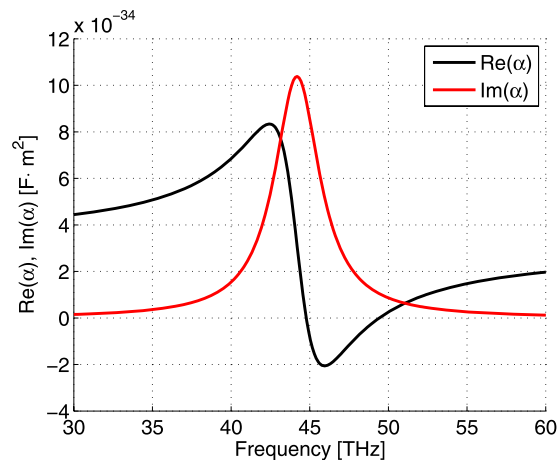
Figure 5. Real and imaginary parts of the polarizability α [F·m^2] of the nanoparticle, made of doped silicon with concentration of carriers 9×10^{19} cm^{-3}.

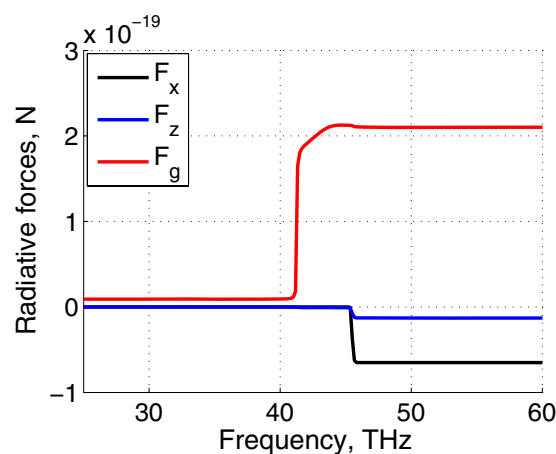**Figure 6.** Radiative forces [N] versus frequency for $h = 400$ nm, $T = 450$ K, and $\phi = 50°$: F_g is the conservative, attractive gradient force, exerted by non-homogeneous fields of evanescent waves (red); F_x (black) and F_z (blue) are the lateral and normal repulsive, non-conservative forces, induced by the corresponding components of the Poynting vector, respectively.

to all forces come from the frequency band 41–45 THz corresponding to the Lorentz resonance for k_z. Further integration does not change the results; saturation is observed after 47 THz.

The normal component of the force consists of contributions from the gradient force, F_g, and the force, caused by the Poynting vector, F_z. One can verify, that at such a distance the van-der-Waals attractive force is comparable with the lateral force. The magnitude of the lateral drag force is even stronger than the repulsive z-directed force. The spectral densities of these forces were calculated and pictured within the frequency range 20 THz–60 THz in which the Lorentz model for orthorhombic boron nitride (27) applies, see Fig. 6. Our estimations thus show that the predicted lateral force could be detected experimentally. Visualization of the velocity of the colloidal nanoparticle could be carried out by using the method of particle image velocimetry successfully employed with gold nanoparticles[33]. Under the influence of this lateral force, the acceleration of the nanoparticle is 2.46 m/s^2. One can expect saturation of the particle speed due to contactless quantum friction. To make that lateral forces are the only ones acting on the particle, one can inhibit the perpendicular Casimir force by placing a non-absorbing layer between the particle and the absorbing layer. In this way, the particle could only move along the lateral direction.

In summary, we have predicted a new effect caused by the fluctuations of the electromagnetic field nearby an absorbing anisotropic slab: the presence of lateral drag forces emerging when the anisotropy axis of the slab is tilted. Electromagnetic fluctuations have been treated within the framework of Rytov's formalism which constitutes one of the important tools to study fluctuation-induced interactions, and it is applicable at the nanoscale as well[5]. This effect systematically occurs in any absorbing anisotropic media, but it may be especially relevant for materials with a strong anisotropy. To prove the existence of such forces, we have solved the boundary value problem in the TM-waves approximation that ignores the hybrid nature of the waves supported by the slab for the considered anisotropy, if $k_y \neq 0$. The presence of these drag forces which can be referred to as "*the driving force from nothing*"[34] can play an important role in the manipulation of nanoparticles close to a surface.

References

1. Volokitin, A. I. & Persson, B. N. J. Rev. Mod. Phys. **79**, 1291 (2007).
2. Casimir, H. B. G. Proc. K. Ned. Akad. Wet. B **51**, 793 (1948).
3. Lamoreaux, S. K. Rep. Prog. Phys. **68**, 201 (2005).
4. Lifshitz, E. M. Zh. Eksp. Teor. Fiz. **29**, 94 (1955) [Sov. Phys. JETP **2**, 73 (1956)].
5. Rytov, S. M. Zh. Eksp. Teor. Fiz. **33**, 166 (1957) [Sov. Phys. JETP **6**, 130 (1958)].
6. Antezza, M., Pitaevskii, L. P., Stringari, S. & Svetovoy, V. B. Phys. Rev. A **77**, 022901 (2008).
7. Lapas, L. C., Pérez-Madrid, A. & Rubi, J. M. Phys. Rev. Lett. **116**, 110601 (2016).
8. Pendry, J. J. Phys.: Condens. Matter **9**, 10301(1997).
9. Volokitin, A. I. & Persson, B. N. J. J. Phys.: Condens. Matter **11**, 345 (1997).
10. Pogrebinskii, M. B. Sov. Phys. Semicond. **11**, 372 (1977).
11. Price, P. J. Physica B + C 117, 750 (2083).
12. Chiu, H.-C., Klimchitskaya, G. L., Marachevsky, V. N., Mostepanenko, V. M. & Mohideen, U. Demonstration of the asymmetric lateral Casimir force between corrugated surfaces in the nonadditive regime. *Phys. Rev. B* **80**, 121402R (2009).
13. Chiu, H.-C., Klimchitskaya, G. L., Marachevsky, V. N., Mostepanenko, V. M. & Mohideen, U. Lateral Casimir force between sinusoidally corrugated surfaces: Asymmetric profiles, deviations from the proximity force approximation, and comparison with exact theory. *Phys. Rev. B* **81**, 115417 (2010).
14. Woods, L. M. *et al. Rev. of Modern Physics* **88**, 045003 (2016).
15. Chen, F., Mohideen, U., Klimchitskaya, G. L., Mostepanenko, V. M. Phys. Rev. Lett. **88**, 101801 (2002).
16. Bimonte, G., Emig, T., Kardar, M. Appl. Phys. Lett. **100**, 0741110 (2012).
17. Rodriguez, A. W., Capasso, F. and Johnson, S. G. Nature Photonics, **5**, 211–221 (2011).
18. Müller, B. and Krüger, M. Phys. Rev. A **93**, 032511 (2016).
19. Veble, G. & Podgornik, R. R. Van der Waals torque and force between dielectrically anisotropic layered media. *Phys. Rev. B* **80**, 075422 (2009).
20. Parsegian, V. A. *Van der Waals Forces*: *A Handbook for Biologists*, *Chemists*, *Engineers*, *and Physicists* (Cambridge University Press, Cambridge, England) (2006).
21. Hashemi, S. M. and Nefedov, I. S. Phys. Rev. B **86**, 195411 (2012).
22. Nefedov, I. S., Valagiannopoulos, C. A., Hashemi, S. M. and Nefedov, E. I. Sc. Rep. **3**, 2662 (2013).
23. Lankaster, P. Theory of Matrices, Academic Press, New York - London (1969).
24. Lifshitz, E. M. and Pitaevskii, L. P. *Statistical Physics: Theory of the Condensed State* (Pergamon, Oxford) (1980).
25. Krüger, M., Bimonte, G., Emif, T. & Kardar, M. "Trace formulas for nonequilibrium Casimir interactions, heat radiation, and heat transfer for arbitrary objects,". *Phys. Rev. B* **86**, 115423 (2012).
26. Messina, R. & Antezza, M. "Scattering-matrix approach to Casimir-Lifshitz force and heat transfer out of thermal equilibrium between arbitrary bodies,". *Phys. Rev. A* **84**, 042102 (2011).
27. Ordin, S. V., Shapurin, B. N. and Fedorov, M. I. Semiconductors **32**, 924–932 (1998).
28. Felinskyi, S. G., Korotkov, P. A. and Felinskyi, G. S. LFNM**2011, 11-th Int. Conf. on Laser and Fiber-Optical Network Modeling, 5–8 Sept., Kharkov, Ukraine, 1–3 (2011).
29. Albaladejo, S., Marqués, M. I., Laroche, M. and Sáenz, J. J. Phys. Rev. Lett. **102**, 113602 (2009).
30. Masetti, G., Severi, M. and Solmi, S. IEEE Trans. on Electron Devices **30**, 764 (1983).
31. Basu, S., Lee, B. J. and Zhang, Z. M. J. of Heat Transfer **132**, 023301 (2010).
32. Markuier, F., Joulain, K., Carminati, J.-P. and Greffet, J.-J. Opt. Commun. **237**, 379 (2004).
33. Fedosov, I. E., Nefedov, I. S., Khlebtsov, B. N. and Tuchin, V. V. Quantum Electron. **38**, 530–535 (2008).
34. Lambrecht, A. "The Casimir effect: a force from nothing", Physics World, 29–32, Sept (2002).

Acknowledgements

Author Contributions

I.N. implemented derivation of formulas and calculations. J.M.R. assisted in the mathematical derivations and was responsible for the physical interpretation. The text of article was written by both authors.

Additional Information

Competing Interests: The authors declare that they have no competing interests.

Publisher's note: Springer Nature remains neutral with regard to jurisdictional claims in published maps and institutional affiliations.